JACS
JOURNAL OF THE AMERICAN CHEMICAL SOCIETY
pubs.acs.org/JACS
Article

Slow Propagation of Ice Binding Limits the Ice-Recrystallization Inhibition Efficiency of PVA and Other Flexible Polymers

Pavithra M. Naullage and Valeria Molinero*

Cite This: J. Am. Chem. Soc. 2020, 142, 4356−4366
Read Online
ACCESS | Metrics & More | Article Recommendations | Supporting Information

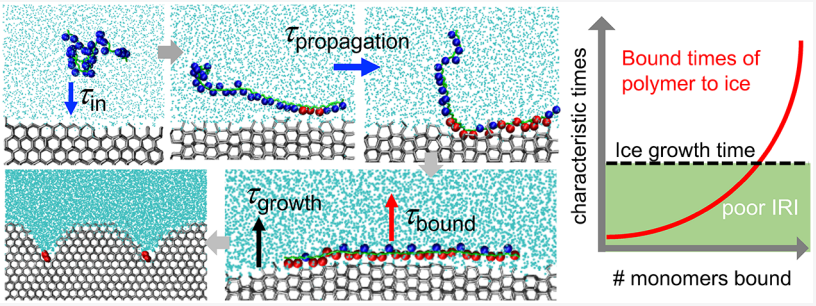

ABSTRACT: Ice recrystallization inhibitors (IRI) are of critical importance in biology, cryopreservation of cells and organs, and frozen foods. Antifreeze glycoproteins (AFGPs) are the most potent IRI. Their cost and cytotoxicity drive the design of synthetic flexible polymers that mimic their function. Poly(vinyl alcohol) (PVA) is the most potent biomimetic found to date, although it is orders of magnitude less potent than AFGPs. A lack of molecular understanding of the factors that limit the IRI efficiency of PVA and other flexible ice-binding polymers hinders the design of more potent IRI. Here, we use molecular and numerical simulations to elucidate how the degree of polymerization (DP) and functionalization of PVA impact its IRI. Our simulations indicate that the onset of IRI activity of PVA occurs for 15 < DP < 20, in agreement with experiments. We predict that polymers with stronger binding to ice per monomer attain IRI activity at lower DP and identify this as a contributor to the higher IRI potency of AFGPs. The simulations reveal that the limiting step for binding of flexible molecules to ice is not the alignment of the molecule to the surface or the initiation of the binding but the propagation to reach its full binding potential. This distinguishes AFGPs and PVA from rigid antifreeze proteins and, we argue, is responsible for their different scaling of efficiencies with molecular size. We use the analysis of PVA to identify the factors that control the IRI activity of flexible polymers and assess the molecular characteristics that endow AFGPs with their exceptional IRI potency.

1. INTRODUCTION

The control of ice recrystallization is central to medical, environmental, and industrial applications ranging from cryopreservation of organs, cellular drug therapy, frozen food, crop damage in agriculture, and ice repellent coatings for infrastructures.[1−17] Ice recrystallization is an Ostwald ripening process in which larger ice crystals grow at the expense of smaller ones.[18−21] The large ice crystals have deleterious effects on organisms, e.g., they can cause mechanical damage to cell membranes and induce osmotic shock.[5,14] Hence, controlling and inhibiting ice-recrystallization is of utmost importance for cryopreservation and biology.

Ice-binding macromolecules such as antifreeze proteins and glycoproteins enable life at subfreezing conditions by preventing the growth and recrystallization of ice.[1,2,22,23] The effectiveness of the ice recrystallization inhibition (IRI) agents depends on their ability to prevent the coarsening of ice crystals with time. Molecules that bind and pin the ice surface create a metastable rippled ice surface that arrests the growth of ice.[24−26] The development of a stationary state depends on a competition between the time scales of binding and unbinding of the IRI molecules to the ice surface and the rate of growth of ice. The latter is controlled by the difference in equilibrium melting temperatures of small and large crystals. For example, according to the Gibbs−Thomson equation for spherical particles, $T_m(R) = T_m^{bulk} - 78\ \text{K nm}/R$,[24,27,28] the difference in T_m between 1 and 2 μm radii ice crystals is ∼0.04 K. The growth rate of ice for that degree of supercooling is 0.02 Å ns^{-1},[29,30] i.e., it takes ∼0.15 μs to build a new ice bilayer. Ice-binding molecules with bound times shorter than the characteristic time to grow ice will be inefficient at stopping its recrystallization.[31]

Antifreeze glycoproteins are the most potent IRI agents.[26,32] However, their industrial use is hindered by synthetic

Received: December 1, 2019
Published: February 13, 2020

https://dx.doi.org/10.1021/jacs.9b12943
J. Am. Chem. Soc. 2020, 142, 4356−4366

challenges such as their cost and possible toxicity.[33,34] Knight et al. found that synthetic mimics of AFGP such as poly(vinyl alcohol) (PVA), poly(L-hydroxyproline), and poly(L-histidine) display ice recrystallization inhibition activity.[35] PVA is the most potent synthetic IRI agent found to date.[33] The high IRI activity of PVA, its low cost, minimal toxicity, and non-penetrative action, make it an excellent candidate for replacing antifreeze proteins (AFP) and antifreeze glycoproteins (AFGP) in cryopreservation, as well as in biomedical and dietary applications.[34,36,37]

PVA prevents ice growth through binding to the prismatic face of ice.[19,24,38,39] Binding of PVA to ice is facilitated by lattice matching between the adjacent hydroxyl groups of the polymer and the water molecules along the *c*-axis of the prismatic plane of ice.[19,38] Because of this, PVA binds ice exclusively along the direction of the *c* axis by adopting a one-dimensional binding configuration.[38,40] Linear binding of PVA to the prismatic plane of ice is also supported by the scanning transmission electron microscopy (STEM) imaging of PVA bound to growing ice, which shows grooves of the same length—about 700 nm—as that of the extended polymer.[41]

Establishing the minimum length of the polymer required for activity is crucial to design synthetic mimics of antifreeze proteins. Budke and Koop conjectured that PVA binds to ice with a minimum of six to eight monomer units.[19] Their experiments were made with commercial PVA that is partially acetylated and has a highly dispersed molecular weight distribution. Gibson and co-workers later investigated the IRI activity of PVA with a well-defined degree of polymerization (DP), which they synthesized using radical polymerization techniques, and they observed a significant increase in the IRI activity with increase in DP.[33] The effect was the most pronounced when the DP increased from 10 to 19.[33] On the basis of these results, they suggested that the minimum repeating sequence required for IRI activity is between 10 to 19 monomeric units.[33] The origin of this threshold has not been established.

PVA can be fine-tuned in-terms of functionalization, opening promising ways of enhancing its antifreeze and ice recrystallization inhibition activities.[25,32,33] Extensive experiments[5,19,20,32,33,42−47] and molecular simulations[24,26,38,48−52] have been performed to understand the structural features that control the binding of molecules to ice. One such modification is the inclusion of hydrophobic groups to IRI agents to improve their potency.[46,47] It has been shown that the addition of hydrophobic groups to *n*-octyl-galactoside increased its IRI activity compared to that of pure galactose.[46] Therefore, it was expected that the IRI activity of PVA would increase upon introduction of hydrophobic groups to the chain.[53] On the contrary, Congdon et al. found that acetylation of PVA reduces its IRI activity.[33] To understand this result, they proposed that the incorporation of acetate groups makes the polymer more hydrophobic, resulting in a more collapsed structure with diminished exposure to water.[33] However, in the same study, they found that the IRI activity of PVA also decreases upon random functionalization with hydrophilic groups.[33] These results suggest that modulations of hydrophobicity are not the main drivers of the IRI activity of ice-binding polymers.

The commonality to hydrophobic and hydrophilic modifications to PVA molecules is the inclusion of moieties that disrupt the continuity of the hydroxyl groups along the PVA chain. It is not yet understood how the presence of modifications in the hydroxyl sequence in the chain affects its binding to ice, e.g., whether they impact the kinetics or thermodynamics of ice-binding. The mechanism by which acetylated PVA binds to ice and its implications for its IRI effectiveness are not known.

Few theoretical models have been proposed to quantify the effect of binding molecules on crystal growth. The kinetic pinning (KP) model of Sander and Tkachenko assumes that ice-binding molecules (IBM) bind irreversibly to ice as they reach the ice surface.[54] According to the KP model, when the rate of adsorption of the IBM is higher than the rate of engulfment of these molecules by the growing ice front, the growth of ice stops. In a recent study, Chasnitsky and Braslavsky (CB) assessed for a wide range of proteins the validity of the KP model, which they modified to consider that the IBMs that arrive to the ice surface have a probability p of binding to ice.[27] CB found that the modified KP model explains well the relationship between the thermal hysteresis (TH) and concentration of IBM for moderately active type III AFP that binds irreversibly to the prismatic plane of ice, while the model fails to account for the TH of hyperactive proteins that bind irreversibly to both the basal and prismatic ice planes.[27] PVA only binds to the prismatic plane of ice, the same as type III AFP. However, it has not been established whether the binding of PVA to ice is irreversible, how the irreversibility depends on the DP of PVA, and how the probability of binding PVA depends on its DP and functionalization.

An alternative model for kinetic inhibition of crystal growth that does not assume reversible binding was proposed recently by Yagasaki, Matsumoto, and Tanaka (YMT) to explain the role of the DP of kinetic inhibitors on the growth of clathrate hydrates.[31] There are two main differences between the KP and YMT models. First, while KP always assumes irreversible binding, YMT assumes that the binding can be reversible for short polymers and increasingly stronger and irreversible for longer ones. Second, YMT does not account for the engulfment of bound molecules by the growing crystal. It assumes that molecules which have a bound time at the surface higher than a threshold value (determined by the intrinsic growth rate of the crystal surface) can halt crystal growth even if they bind reversibly to the surface.[27] The relationship between the DP of PVA and the time the oligomers remain bound to the ice surface is not known.

In this study, we use large-scale molecular dynamic simulations with computationally efficient united atom models[38,55] to first unravel how PVA molecules with different degrees of polymerization bind to the ice surface and then discern how long they remain bound. We then use molecular and numerical simulations to elucidate how the acetylation of PVA impacts the ice binding and its IRI activity. Our results and analysis point to important differences in the size-dependence of the ice-binding efficiency of flexible and rigid ice binding molecules, and to the important role that the time scale of propagation of the binding across the chain has on the efficiency of flexible ice-binding polymers. We use these insights to assess the factors that endow AFGPs with their exceptional IRI activity and to identify ways to increase the IRI efficiency of synthetic polymers.

2. RESULTS AND DISCUSSION

Effect of Chain Length on IRI Activity. We investigate the effect of the polymer length on ice binding by performing simulations of PVA with DP = 6, 10, 15, 20, and 30 in

https://dx.doi.org/10.1021/jacs.9b12943
J. Am. Chem. Soc. 2020, 142, 4356−4366

simulation cells where the prismatic plane of ice is in equilibrium with liquid water at 273 K, the melting temperature of ice in the mW water model.[55] The details of the simulations and the order parameters used for identifying whether PVA is bound to ice are discussed in the Methods section.

Figure 1 illustrates the process of binding of PVA with DP = 30 to the prismatic face of ice. The simulation shows that the binding is not immediate, despite the small volume of liquid available to the molecule. There are multiple binding attempts in which the molecule binds ice through no more than ~3 OH groups and almost immediately unbinds. Only when PVA binds through more than ~8 OH groups, the binding becomes irreversible in the hundreds of nanoseconds time scale of the simulations.

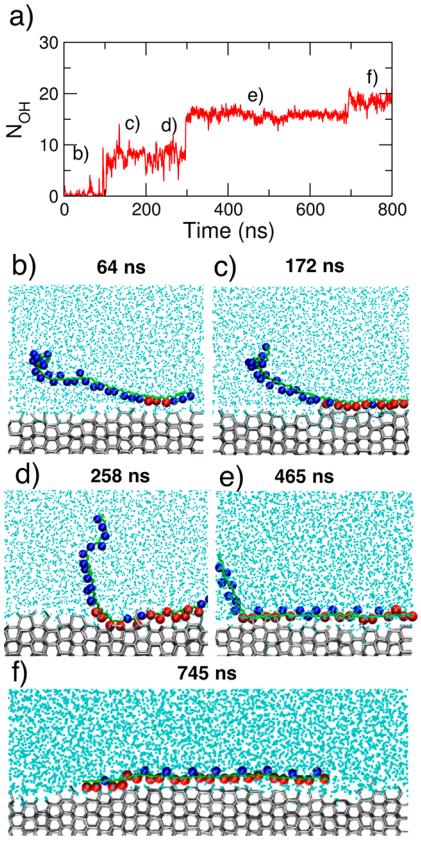

Figure 1. PVA with DP = 30 binds to the prismatic plane of ice in a long process that is reversible at its early stages. (a) Time evolution of the number of OH groups of PVA bound to ice, N_{OH}, where N_{OH} is computed as a running average over 1 ns windows of the trajectory to filter fast fluctuations that do not physically correspond to binding/unbinding events. (b–f) Snapshots along the binding simulation. The times corresponding to the snapshots are indicated in panel a. Ice is represented with silver sticks, water with cyan points, bound OH groups of PVA with red balls, unbound OH groups with blue balls, and the hydrocarbon backbone with green sticks.

The simulation trajectory of PVA with DP = 30 in Figure 1 illustrates features we see in the binding to ice of PVA oligomers of all lengths: the binding starts at a random position of the chain, it is reversible over hundreds of nanoseconds when the number of OH bound is less than ~10, and the propagation of the binding typically proceeds in discrete "bursts" in which consecutive monomers of PVA bind to the ice surface over a short time period of, typically, 3 to 15 ns, separated by long waiting times during which a combination of the fluctuations of the ice surface and the orientation of the chain hinders the propagation of the binding. We observe the same mode of binding for PVA with DP = 6, 10, 15, and 20 (results for representative trajectories shown in Figure 2, full sets in SI Figures S1–S3). We find that defects on the ice surface slow down the binding and propagation of PVA on ice. We expect this also to be the case for curved ice surfaces, because PVA binding is specific to a particular direction of a specific plane of ice. We conclude that even when PVA is *at* the ice-liquid surface, it has to surmount several barriers to fully bind to ice. These processes result in a low probability of binding, even for those chains that are long enough to eventually attach irreversibly to the ice surface.

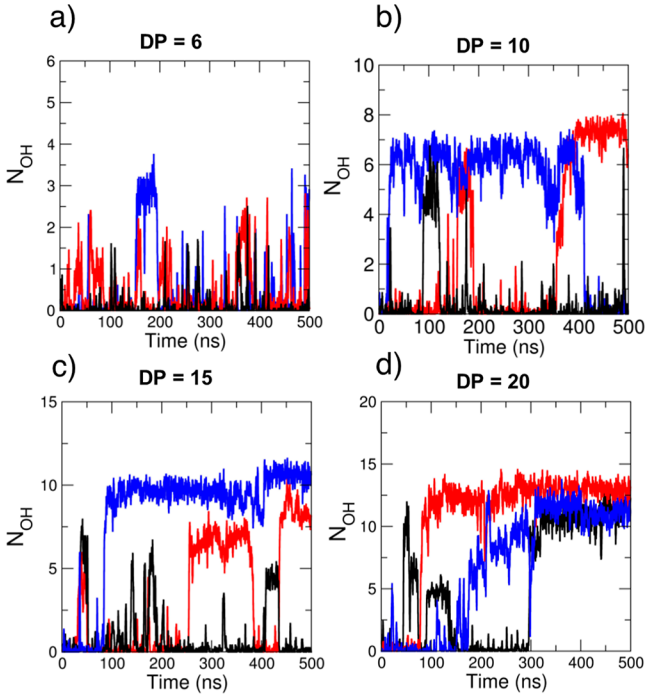

Figure 2. Time evolution of number of bound OH groups of PVA, N_{OH}, for representative ice-binding trajectories of oligomers with (a) DP = 6, (b) DP = 10, (c) DP = 15, and (d) DP = 20. The full set of trajectories for DP = 10, 15, and 20 is shown in SI Figures S1–S3. Similar to Figure 1, N_{OH} is the running average over 1 ns windows of the instantaneous number of OH bound. The maximum N_{OH} is ~2/3 of the DP, due to 2 bound:1 unbound binding pattern of PVA.[38]

We analyze the complete set of binding simulations of PVA oligomers to compute the bound times τ of each oligomer at the ice surface as a function of the average number n_{OH} of OH groups bound for that time interval. The results are summarized in Figure 3. We find that τ depends on n_{OH} but not on the degree of polymerization of PVA. The higher the DP of PVA, however, the higher is the number of OH groups that can bind to ice and the longer is the maximum time that the chain can pin the ice surface, preventing its growth.

Figure 3 points to an increase in the bound time with the number of OH of PVA bound to the ice surface that is slightly higher than exponential. An exponential increase would be consistent with the YMT model,[31] which assumes that the binding free energy grows linearly with the number of bound groups, $\Delta G_{bind} = \Delta G_{OH}\, n_{OH}$, where ΔG_{OH} is the binding free

https://dx.doi.org/10.1021/jacs.9b12943
J. Am. Chem. Soc. 2020, 142, 4356–4366

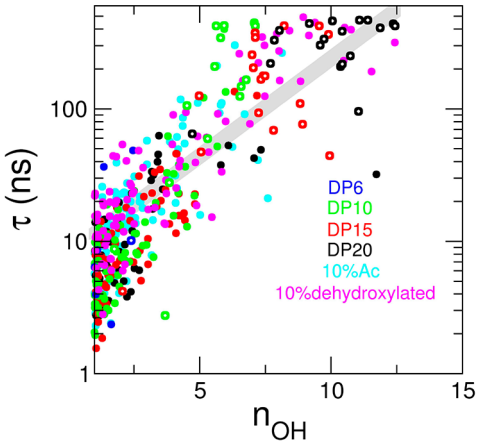

Figure 3. Bound time τ of PVA at the ice surface increases exponentially with the average number of OH groups bound to ice, n_{OH}, irrespective of the DP of the polymer and its functionalization. The data for DP = 6 are shown in blue (from 3 × 0.5 μs simulations), for DP = 10 in green (from 20 × 0.5 μs simulations), for DP = 15 in red (from 20 × 0.5 μs simulations), for DP = 20 in black (from 20 × 0.5 μs simulations), for 10% acetylated PVA with DP = 30 in cyan (from 10 × 1 μs simulations), and for 10% dehydroxylated PVA with DP = 30 in magenta (from 20 × 0.5 μs simulations). The open circles correspond to the last bound time for each simulation trajectory, limited by the running time and not unbinding of the molecule. Gray line is obtained by fitting all bound times between 1 and 100 ns in the graph to $\tau = \tau_o \exp(\Delta G_{OH} n_{OH}/RT)$, which results in τ_o = 8.1 ns and ΔG_{OH} = 0.77 kJmol^{-1}.

energy per monomer, and that the bound time of the molecule at the surface is $\tau = \tau_o \exp(\Delta G_{OH} n_{OH}/RT)$. If we assume an exponential increase in τ with n_{OH}, we obtain τ_o = 8.1 ns and ΔG_{OH} = 0.77 kJmol^{-1} by fitting to this equation the bound times between 1 and 100 ns collected for all polymers in Figure 3. The fit is shown with a gray line in the figure. The ΔG_{OH} obtained from the fit is a lower bound to the real value, even more than the figure shows, because the bound times for the largest n_{OH} are limited by the simulation times and not the detachment of the chains from the ice surface. Cooperativity due to distinct scaling of the enthalpy and entropy of binding[38] may be the origin of the faster than exponential increase we cannot resolve with the data of Figure 3. Table 1 shows the

Table 1. Average Residence Times of PVA Oligomers Fully Bound to Ice Predicted by τ_o = 8.1 ns and ΔG_{OH} = 0.77 kJmol^{-1}[b]

DP	6	10	15	20	30
$\tau_{\text{fully bound}}$[a] (ns)	30	80	250	760	7400

[a]Compare with 0.15 μs time scale for growth of ice bilayer under typical IRI conditions. The capping of long bound times by the simulations times in Figure 3 suggests that for DP > 10, the bound times may increase more steeply with DP than indicated by our fitting. [b]Obtained by fitting data in Figure 3 and considering that fully bound PVA binds through 2/3 of its OH groups.

predicted bound times of PVA oligomers fully bound to ice using this fit, where we have considered that n_{OH} of the fully bound chain is 2/3 of its DP, according to the 2 bound:1 unbound binding pattern of PVA,[38] using the parameters of the gray fitted line of Figure 3. A comparison of the bound times of PVA of different DP and the 0.15 μs it takes to grow an ice bilayer under typical IRI conditions explains why the experimentally observed IRI activity of PVA increases significantly when DP increases from 10 to 19.[33]

Our analysis indicates that there are three main factors that control the efficiency of flexible polymers as IRI. First, the strength of their ice-binding free energy per site, which determines the bound times per number of monomers adsorbed to ice. Second, the length of the polymer, which combined with the binding strength per monomer sets the maximum bound times of the polymer pinning the ice-surface. Third, the rate of propagation of the binding of the polymer to ice, which in conjunction with the binding free energy per site determines the probability that a polymer that starts binding to ice undergoes a long series of reversible binding/unbinding events before reaching its full binding potential. To our knowledge, the time of propagation of the binding has not been previously considered in the analysis or design of ice-binding molecules. In next section, we show that it plays a key role in the drop in IRI efficiency of PVA upon acetylation.

Effect of Polymer Functionalization on IRI Activity. Experiments indicate that the random acetylation of long PVA chains has a dramatic effect on their performance as IRI. For example, 30% acetylation completely obliterates the IRI activity of PVA with DP_{total} = 351.[33] This poses the question of why this PVA copolymer with 245 OH groups is unable to stop the recrystallization of ice: is the depression of the IRI upon functionalization the result of thermodynamic or kinetic effects?

It has been proposed that the replacement of hydroxyl groups by the more hydrophobic acetyl groups makes PVA more compact, decreasing its ability to bind to ice.[33] This could be a contributor to the lower IRI of acetylated PVA. In our simulations, however, we purposefully exclude the effect of increased compactness by tuning the interaction strength between the carbonyl group and water to result in the same radius of gyration for acetylated and nonacetylated PVA. This allows us to focus on how the IRI is impacted by the disruption of the polymer's binding sequence.

We first study the effect of acetylation on PVA binding to ice by *systematically* acetylating 20% or 10% of the monomers in a chain with DP_{total} = 30, i.e., one every five or one every ten hydroxyl groups are acetylated. This results in copolymers with blocks of PVA of uniform DP = 4 and 9, respectively, separated by PVAc blocks of DP = 1. We evolve one simulation of PVA with 20% acetylation and ten simulations for PVA with 10% acetylation. Each of these 11 simulations is sampled for at least 1 μs, while we monitor the number of OH groups bound to ice.

Our simulations reveal large barriers for the propagation of the binding to ice through the acetylated monomers: the binding does not propagate over the acetylated monomers in the microsecond time scales of the simulations. An analysis of the bound N_{OH} for each of the three PVA blocks of the 10% acetylated DP_{total} = 30 copolymer (Figures 4 and S4) indicates that the acetylated chain behaves similarly as PVA with DP = 9, the length of its pure PVA blocks. Likewise, the 20% acetylated PVA behaves as PVA with DP = 4 (Figure S5). We conclude that the acetylated monomers decrease the bound times of PVA and its IRI efficiency by interrupting the propagation of the binding of the polymer to ice.

The 10% acetylated chain sometimes binds ice through OH groups in multiple PVA blocks (Figures 4 and S4). Most of these cases result in unbinding of the chain, consistent with the low bound time for DP = 9 (Table 1 and Figure 3). However,

https://dx.doi.org/10.1021/jacs.9b12943
J. Am. Chem. Soc. 2020, 142, 4356−4366

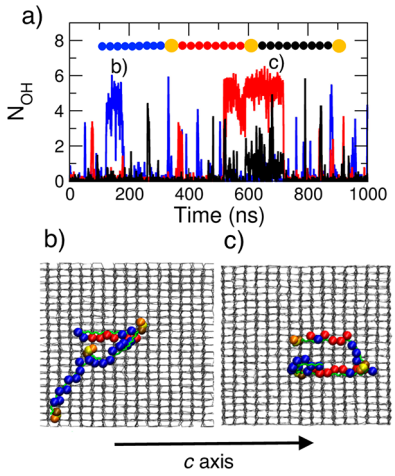

Figure 4. Acetyl groups separate the PVA chain into independent segments from the point of view of their binding to ice. (a) Time evolution of the number of OH groups bound to ice, N_{OH}, for each segment of the polymer separated by the acetyl group for a 10% acetylated PVA. The blue, red, and black lines correspond to the first middle and last blocks of the polymer, respectively, as sketched in the inset of panel a. Binding starts randomly at any of the three unfunctionalized blocks, and the propagation occurs linearly along the *c*-axis of the ice plane, the same as that for the unfunctionalized PVA, but it stops before reaching the acetylated monomer. (b, c) Snapshots of the system at the times indicated with letters b and c in panel a. The snapshots depict ice with silver sticks, the hydrocarbon backbone of PVA with green sticks, its bound OH groups with red balls, and its unbound OH groups with blue balls. The ester oxygen, carbonyl oxygen, and carbonyl carbon of the acetylated monomers are shown with brown, yellow, and orange balls, respectively. Liquid water is not shown, for clarity.

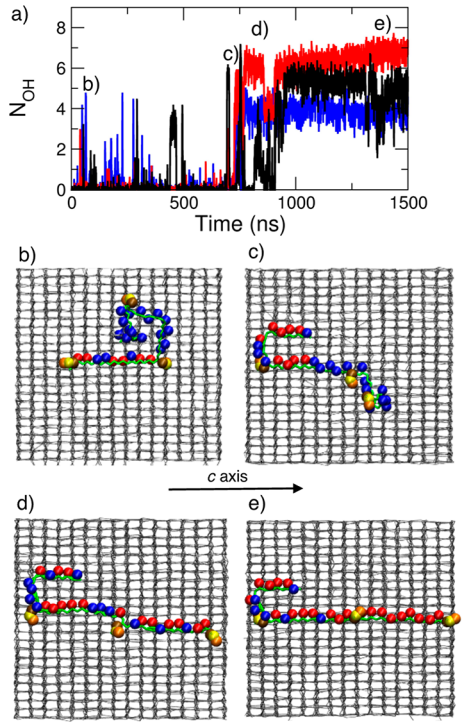

Figure 5. Independent binding of PVA blocks of acetylated PVA can lead to a fully bound PVA/PVAc at the ice surface. (a) Time evolution of the number of bound OH of each PVA block of 10% acetylated PVA. The three lines indicate the PVA blocks; same colors as in Figure 4. (b–e) Snapshots along the simulation depicting the rearrangement of the bound polymer segments that leads to a fully bound 10% acetylated PVA on the ice surface. The times corresponding to the snapshots b to e are indicated in panel. Colors are same as in the snapshots of Figure 4. Note that in panel e, the small size of the simulation cell precludes the full extension of the molecule on the surface.

we found a case, shown in Figure 5, in which independent binding of multiple PVA blocks was followed by molecular rearrangements that allowed the chain to adopt an aligned linear conformation that maximized the number of OH groups bound to ice. The final state does not unbind from ice over hundreds of nanoseconds (Figure 5). This indicates that the difficulty of acetylated PVA to bind ice is not due to a significant destabilization of the bound state, but it rather arises from large kinetic barriers for the propagation of the binding across PVA blocks of the copolymer.

To understand the origin of the large barrier for propagation of binding over the acetylated monomers, we assess the effect of the functionalization on the dihedral distribution of the alkyl backbone of the polymer, as these dihedrals control the orientation of the unbound chain with respect to the ice-binding axis. The alkyl backbone has two preferred dihedrals: the $\phi \approx \pm 180°$ trans conformation and the $\phi \approx \pm 60°$ "kinked" one. Only the trans conformation is conducive to the 1D-binding of PVA to ice. We find that dihedrals that involve an acetylated carbon have an increased population of kinked conformations for the polymer in solution (Table 2). For example, the C–C–C–C torsion around the acetylated C carbon is 56% of the time in the kink conformation, compared to 14% for the C–C–C–C dihedral of pure PVA in water. The fraction of kinked conformations for the C–C–C–C dihedral of pure PVA bound to ice is even lower, 4% (Table 2). The preference for kinked conformations in the torsions that include the acetylated monomer in solution and bound to ice (Table 1) may contribute to the barrier of propagation over them. However, it cannot be its sole origin, because the

Table 2. Percentage of Backbone Dihedrals in Kink Conformations, $\phi \approx \pm 60°$[a]

dihedral	% kink dihedral in solution	% kink dihedral bound to ice
C–C–C–C	14	4
C–C–C–C	40	31
C–C–C–C	56	30

[a] C is the backbone carbon of an acetylated monomer.

dihedrals involving the acetylated monomer can remain in the trans conformation for more than hundred nanoseconds (Figure S6), a time that would be sufficient for the propagation of binding of pure PVA. We conjecture that steric hindrances between the acetyl groups and ice may also contribute to the barrier for propagation of the binding.

To test our hypothesis that the barriers for binding over the acetylated monomers originate on steric effects and not from the discontinuity in the sequence of the OH groups, we investigate the binding of a polymer in which we remove some OH groups instead of replacing them with bulkier groups. As the systematic removal of one of every 3 OH groups may not impact the binding of PVA, because of its 2 OH bound:1 OH unbound pattern,[19,38] we prepare a 10% dehydroxylated PVA copolymer by removing one of every 10 OH groups in a DP = 30 PVA, forcing the binding to miss at least one OH group and investigate its mode of binding along 20 simulations, each 500 ns long. We find that the 10% dehydroxylated chain binds to

https://dx.doi.org/10.1021/jacs.9b12943
J. Am. Chem. Soc. 2020, 142, 4356–4366

ice in almost the same way as PVA of the same length, extending linearly over the ice. The absence of the OH group does not have a noticeable impact on the time scale of propagation of the binding (Figure S7). We conclude that acetylation of PVA hampers the binding to ice through steric effects and not by introducing discontinuities in the OH sequence along the chain.

Our analysis above indicates that acetylation of PVA separates the chain into quasi-independent ice-binding fragments. This explains why block copolymers of PVA and non-ice-binding monomers have the IRI activity of the PVA block.[56] To understand the dramatic effect that a random distribution of acetyl and other non-ice-binding groups have on the IRI activity of PVA,[33,56] we combine the above results and insights of the molecular simulations of PVA and regularly acetylated PVA with numerical analyses of the distribution of the lengths L of uninterrupted PVA sequences in statistical copolymers.

The probability $p(L)$ of finding a PVA block of length (i.e., DP) L in the randomly acetylated polymer decays exponentially with L (Figure S8). The probability that the binding occurs through a PVA block of length L, however, increases with L, because binding can start from any OH along the chain. Hence, the most probable length of the PVA block that binds to ice is given by the maximum in the product of the length L and its probability, $L \times P(L)$, shown in Figure 6a: the most probable number of OH groups in the ice-binding block decays from 18 to 3 as the acetylation increases from 5% to 30%.

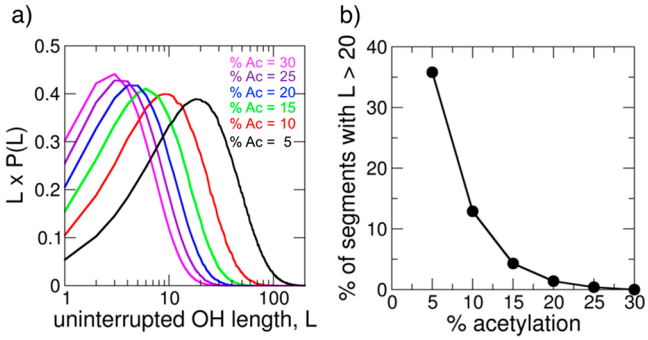

Figure 6. Length L of the PVA block that contains the most probable binding site decays steeply with increasing acetylation of the chain. (a) Distribution of the most probable length of uninterrupted PVA for different % acetylation. (b) Percentage of PVA blocks in randomly acetylated polymers that have DP ≥ 20 decays from 36% to 0.1% when the acetylation increases from 5% to 30%. The results given here are for polymer of DP_{tot} = 351. SI Figure S9 shows that $P(L)$ is essentially independent of polymer length if the DP is comparable or larger than the length L corresponding to the tail of the distribution.

IRI experiments[33] and our simulations concur that only PVA segments with DP ≥ 20 bind to ice for times long enough to effectively hold its recrystallization. The percentage of PVA blocks with DP ≥ 20 in the statistical polymer falls exponentially with acetylation, from 36% in the 5% acetylated polymer to just 0.1% in the 30% acetylated one (Figure 6b). Together with the insurmountable barriers for propagation of the binding over acetylated monomers, this explains the steep decrease of IRI activity of PVA with more than 20% acetylation and its complete elimination when the acetylation is ≥30%. We conclude that any structural modification that introduces a barrier for the propagation of ice-binding decreases the efficiency of polymeric IRI agents to those of much shorter versions of the same ice-binding polymer.

3. CONCLUSIONS AND OUTLOOK

Halting of the growth and recrystallization of ice is a challenge that is central to a myriad of medical, environmental, and industrial applications. Burgeoning demands in these areas call for synthetic alternatives that can mimic the potent IRI activity of AFGPs. All synthetic AFGP mimics are polymers, which provide high versatility through changes in architecture and functionalization.[33,46,57] These synthetic polymer mimics are flexible molecules, like AFGPs themselves.[58] Poly(vinyl alcohol) (PVA) is the most effective synthetic mimic of antifreeze glycoproteins.[33] Its IRI effectiveness, however, strongly depends on the degree of polymerization and functionalization of the chain.[33,56] In this work, we use molecular and numerical simulations to elucidate the molecular origin of these dependences. To our knowledge, this is the first molecular simulation study to investigate how the length of the polymer and presence of functional groups affect the efficiency of any ice recrystallization inhibitor.

We find that flexible polymers can initiate the binding to ice from any segment of the chain and that this initiation occurs readily when the polymer is at the ice surface. Our simulations reveal that the limiting step for flexible polymers is the *propagation* of the binding to the ice surface. Capillary fluctuations of the ice surface and the segmental dynamics of the chain control the time of propagation of the binding of the polymer to the ice surface. As the segmental dynamics for polymers in good solvents is independent of the DP,[59] we conclude that the rate of propagation of the ice-binding of any flexible polymer in a good solvent, such as PVA in water, is independent of its degree of polymerization.

While the propagation time is independent of the DP, the time the polymer stays bound to ice increases very steeply with the number of monomers bound. For example, we show that PVA bound by less than ∼6 OH groups detaches from the ice surface in time scales that are short compared to those of ice growth. This results in multiple reversible partial binding events before the polymer can attach through enough OH groups to remain bound to the surface for times that suffice to stop the recrystallization of ice.

The simulations indicate that the bound times of PVA to ice increase faster than in an exponential manner with the number of monomers bound, N_{bound}. This is consistent with a cooperative mechanism in which the free energy of binding increases faster than in a linear manner with N_{bound}, due to a different scaling of the enthalpy and entropy of binding.[38] Flexible polymers that can bind to the crystal in any direction, as is the case for AFGPs,[52] would retain more of the configurational entropy of the chain, resulting in lower cooperativity. If there is no cooperativity in the binding, or if the binding free energy per monomer is large compared to the loss of configurational entropy of the chain upon binding, the bound times would increase exponentially with N_{bound}. Indeed, an analysis of experimental bound times of AFGPs to ice suggested that binding of this flexible polymer is non-cooperative, consistent with the multiple modes of binding of the protein to ice and its retention of flexibility in the bound state.[52] In all cases, irrespective of the degree of cooperativity of the binding, the rate at which the sites bind to the surface (i.e., the propagation time) is the one that controls the

https://dx.doi.org/10.1021/jacs.9b12943
J. Am. Chem. Soc. 2020, 142, 4356−4366

reversibility of the binding and the overall recrystallization inhibition efficiency of flexible molecules. Our analysis indicates that the slow propagation of the binding of flexible polymers diminishes their IRI efficiency because it allows for reversible unbinding of the chain before it reaches its full binding potential. We conclude that the competition between the propagation and bound times of flexible ice binding polymers at the ice surface is key in determining their effectiveness as IRI.

Experiments indicate that long PVA chains are more efficient ice recrystallization inhibitors than short ones when compared at the same molar concentration.[33] We show that this is because the time PVA remains bound to the ice surface increases faster than in an exponential manner with its degree of polymerization, and molecules must remain bound to ice for times that are long compared to the time scales of growth of ice to be effective IRI. Our analysis shows that the bound times of PVA with DP = 10 are shorter than those of ice growth, while those of PVA with DP = 20 are significantly longer. This explains the steep increase in IRI activity in experiments with PVA when the DP increases from 10 to 20.[33] Design polymers with stronger ice-binding free energies per monomer would result in higher probability of binding, less reversibility, and more IRI potency at lower DP. This could be achieved by designing monomers that can bind through multiple OH groups positioned at distances consistent with those of water molecules in an ice plane[38] or through the synergistic use of hydrogen-bonding and hydrophobic interactions.[60]

Ice recrystallization experiments are usually performed with concentrated sucrose solutions.[32,57,61] The time scales of diffusion of the polymer to the ice surface, segmental dynamics of the polymer chain, unbinding of the polymer from ice, and growth rate of ice are all proportional to the viscosity of the medium, which is an order of magnitude higher for 50% sucrose solution than pure water.[62] This implies that IRI of an ice-binding polymer in sucrose solutions, or the interior of a cell, will follow the same mechanism discussed here for pure water, with the time scales of recrystallization extended according to the ratio of the viscosities. We expect the competition between propagation and bound times that determines the effectiveness of IRI molecules to be rather insensitive to the viscosity of the solution containing the ice crystals.

Random acetylation of PVA is known to dramatically decrease its IRI efficiency.[33] We find that binding of acetylated PVA that has tens of hydroxyl groups is thermodynamically favorable. The simulations reveal that the limitation for the binding of acetylated PVA is kinetic: acetylated monomers impose large barriers for the propagation of the binding of the polymer at the ice surface. As we do not find noticeable propagation barriers over non-ice-binding dehydroxylated monomers, we conclude that the barrier for propagation does not arise from discontinuities in the OH pattern of the chain but from the steric hindrance of the acetyl groups.

The insurmountable barriers for propagation of ice binding over acetylated monomers make the bound times of acetylated PVA equivalent to those of short PVA blocks. Binding of acetylated PVA can start at any random OH of the chain, but only blocks with DP $\geq$ 20 can ensure that the binding will be irreversible in the time scales of growth of ice. We demonstrate that the fraction of PVA blocks with DP $\geq$ 20 falls exponentially with the acetylation of the chain. Our analysis explains the dramatic impact of acetylation on the IRI activity of the PVA polymers.[33] We conclude that control over the polymer functionalization and chemistry is key in the design of effective ice recrystallization inhibitors.

Although PVA is, to date, the most efficient synthetic ice recrystallization inhibitor, antifreeze glycoproteins from fish are orders of magnitude more potent IRI than PVA. For example, AFGP8, the smallest antifreeze glycoprotein, can prevent the recrystallization of ice already at a concentration of 0.38 μM,[61] while ten times more concentrated solutions of PVA with DP = 351 are needed to achieve the same IRI activity.[33] In what follows, we discuss what makes the AFGP much more efficient than the most potent synthetic IRI.

AFGP8 is not only much smaller than PVA_{351} (2.65 vs 15.44 kDa, respectively) but also has less ice-binding sites. PVA_{351} can bind ice through ~230 OH groups (i.e., 2/3 of its DP), each contributing about 0.8 $kJmol^{-1}$ to the free energy of binding to ice. AFGP8 binds ice by adsorption of methyl or methylene groups onto the rings of the prismatic face of ice.[52] This glycoprotein has 16 potential binding groups, not all of which can bind simultaneously to ice.[52] The ice-binding free energy per methyl group was estimated to be about 2 $kJmol^{-1}$.[52] While the binding may be stronger due to other interfacial contributions and the adsorption of the protein to ice steps,[52,63] it would have to be at least ~6 times larger to account for the difference in IRI activity between the small AFGP8 and the large PVA_{351} just in terms of the bound times when these molecules are fully adsorbed to the ice surface. This suggests that the stronger ice-binding per site is not the only reason why AFGPs are so potent IRI agents.

Other factors may increase the IRI potency of AFGPs compared to PVA. First, PVA ice binds exclusively along the *c*-axis of the prismatic plane,[19,38] while molecular simulations indicate that AFGP8 binds the prismatic plane in multiple directions.[52] Second, molecular simulations indicate that AFGP8 can "walk" on the ice surface, which would allow them to reach a step where they can adsorb more strongly.[52] The one-dimensional binding of PVA to ice would require a concerted move for the molecule to walk the surface. We have not seen PVA walking the ice surface even in microsecond and longer simulations. Third, PVA adopts a random coil conformation in water that must be extended to bind to ice, resulting in an entropic penalty.[38] AFGP8 has a well-defined secondary structure with the sugar and hydrophobic groups spatially segregated.[52,58] The distances between the hydrophobic ice-binding groups in the native conformation of the peptide of AFGP8 match those of the water rings in the ice surface, facilitating the propagation of the binding.[52] As the binding free energy per ice-binding site of AFGP8 is at least 2.5 times stronger than for PVA, adsorption of at most 5 methyl groups of the AFGP to ice would provide the same binding free energy as the fully bound PVA_{20}, which remains at the ice surface for times long compared to those of ice growth. Fourth, the bulkiness of the AFGP pinned to the ice surface provides a higher resistance for engulfment by the growing ice front, compared to that of the skinny PVA molecule. Our analysis suggests that the stronger binding per site, coupled to the secondary structure that favors propagation of the binding, and the bulkier structure of the AFGP that delays engulfment is responsible for the exceptional IRI activity of AFGPs.

The antifreeze protein of *Tenebrio molitor*, *Tm*AFP, is one of the most potent antifreeze and ice-recrystallization inhibitor.[5] Different from the flexible AFGPs, *Tm*AFP is a rigid beta helix.[48,50,64,65] Ice binding by *Tm*AFP involves a slow diffusive

https://dx.doi.org/10.1021/jacs.9b12943
J. Am. Chem. Soc. 2020, 142, 4356−4366

search in its orientation with respect to the ice surface, until it aligns its long axis to be parallel to one of the *a* axes of the basal plane.[50] Then, the protein binds ice all at once within a few nanoseconds.[50] This indicates that different from flexible polymers, the binding to ice of rigid molecules is limited by the alignment of the molecule with respect to the ice-binding axis of the ice surface and not by the time of propagation.

We argue that the difference between alignment-control of ice binding by rigid molecules vs propagation-control for flexible ones results in different scaling of ice-binding efficiencies with size. The antifreeze activity of engineered *Tm*AFP with $N = 6$ to 11 ice-binding amino acid loops is non monotonous with N, with maximal antifreeze activity for $N = 9$.[66] It has been proposed that the decrease in activity results from an accumulation of mismatch between protein and ice that reduces the ice-binding strength for longer proteins.[66] However, a recent study indicates that the binding strength per monomer does not decrease with the number of coils.[67] Recent analysis by Peters and co-workers demonstrates that the probability of binding rigid rod molecules to ice decreases with increasing length.[68] This suggests that the nonmonotonous antifreeze activity of the engineered proteins is a result of the competition between opposing trends of increasing bound times and decreasing binding probability with increasing number of ice-binding loops. This points to a significant difference in the strategies for optimizing the size of rigid and flexible ice-binding molecules.

The inhibition of ice growth and recrystallization by ice-binding molecules is a complex multistep process. First, the molecule has to be soluble in water—so that enough of it can reach the ice-liquid interface from the solution—but not so comfortable in liquid water that it does not bind to ice; this may be the reason why many ice-binding molecules are amphiphilic. Second, it must diffuse to the ice−water interface; the larger the hydrodynamic radius of the molecule, the slower is this step.[27] Third, the molecule has to bind to the ice surface and remain there for times that are long compared to those of ice growth. This is the step we address in this work. Finally, the molecule has to prevent or delay its engulfment by the growing ice front;[54] this is controlled by the bulkiness of the molecule and the icephobicity of its non-ice-binding site.[24] A quantitative prediction of the ice recrystallization inhibition and antifreeze activity of molecules requires that all these steps are integrated into a common modeling framework. The development of such a multiscale model will facilitate the *de novo* design of synthetic mimics that could match and even surpass the ice recrystallization inhibition of the most potent proteins.

4. METHODS

Simulation Method. We perform molecular dynamic (MD) simulations using LAMMPS.[69] We integrate the equations of motion with the velocity Verlet algorithm using a time step of 5 fs. We build simulation cells that are periodic in the three Cartesian directions. Ice-binding simulations are performed with two-phase systems in the isobaric isoenthalpic ensemble (NpH) at 1 bar, preceded by equilibration of the system in the isobaric isothermal (NpT) ensemble at 273 K and 1 atm. The pressure and temperature are regulated with Nose-Hoover thermostat and barostat[70,71] with time constants 2.5 and 12.5 ps, respectively. The pressure is controlled independently in each direction, except for the one-phase simulations used to compute the dihedral distributions, where a single barostat was used to control the pressure in all directions and the temperature is set to 308 K.

Molecular Models and Force Fields. We model water with the monatomic water model mW in which water is represented by a single particle that interacts through short-range two-body and three-body interactions that mimic hydrogen bonds.[55] The equilibrium melting temperature of hexagonal ice in the mW model is $T_m = 273 \pm 0.5$ K.[72] The mW model has been extensively validated to reproduce the structure,[55,72−75] thermodynamics,[55,72,73,76−81] interfacial properties,[26,55,72,82−94] and phase transitions of water[28,55,74,76,81,92,95−112] as well to model the interactions between ice binding molecules at the ice−water interface.[24,26,38,48,50−52,60,67,113]

We model PVA with the united atom (UA) model compatible with the mW model, introduced in references 24,26,38. As the UA model of PVA does not have hydrogen atoms, it does not have a defined tacticity, although the model was parametrized to reproduce the experimental radius of gyration of atactic PVA.[38] A recent all-atom simulation study found that the mode of binding of PVA 20-mer is independent of its tacticity.[39] Table S4 lists the UA types of the acetyl model. Equations S1 and S2 list the forms of the bonds, angles and dihedrals, and Tables S1, S2, S5, S6 their parameters. The form and parameters of the nonbonded interactions are listed in Tables S3 and Tables S7 and S8.

Systems. The molecules considered in this study are linear PVA oligomers with DP = 6, 10, 15, 20, and 30. Acetylated PVA with DP = 30 contains 10% and 20% acetyl groups uniformly distributed along the chain. The dehydroxylated PVA molecules with DP = 30 have 10% of the hydroxyl groups removed, also uniformly along the chain. We prepare two-phase ice−water systems in which the primary prismatic plane of ice is exposed to liquid water containing a single PVA molecule. The simulation cells exposing the prismatic plane have dimensions 9.4 nm × 5.4 nm × 5.7 nm and contain 9216 water molecules for the studies with DP = 6, 10, 15, 20, and 30. To facilitate the complete binding of the DP = 30 polymer, we continue the simulations with a box of dimensions 9.2 nm × 5.3 nm × 11.4 nm, with 18432 water molecules, obtained by replicating the previous cell in the direction along the *c*-axis of ice, and deleting the PVA image. Simulation cells that contain acetylated PVA with 10% and 20% acetyl groups have dimensions 9.4 nm × 5.3 nm × 5.7 nm and contain 9216 water molecules. The two-phase simulation cells contain approximately the same number of water molecules in the liquid and ice phases. The PVA molecules are initially placed and equilibrated in the liquid phase. The simulations are evolved for times spanning from 500 ns up to 1.5 μs, during which we monitor the binding of PVA to ice. The one phase simulation cell used to compute the dihedral distributions has dimensions of 9.4 nm × 5.4 nm × 5.7 nm with 9216 water molecules and is run for 500 ns.

Identification of Hydroxyl Groups Bound to Ice. We use the CHILL+ algorithm[114] to identify ice and OH groups bound to ice in our systems. The CHILL+ algorithm is accurate at identifying cubic and hexagonal ice from liquid water.[114] We identify the OH groups to be bound to ice when an OH group is within 6 Å of either hexagonal or cubic ice. That distance accounts for the existence of a layer of interfacial ice[96,114] between the ice-binding molecule and the surface. The time evolution of the OH groups bound, N_{OH}, contains fast variations that arise due to the fast fluctuations of the ice surface and vibrations of the polymer that do not lead to unbinding. We filter out the fast fluctuations in the order parameter by taking running average over 1 ns windows along the simulation trajectories.

Computation of Bound Times. We compute the bound times, τ, of PVA with different DP as the time each PVA molecule stays bound to the ice surface. The start and end of these periods are signaled by $N_{OH} = 0$, except for the last bound period of the trajectory, where we collect the total time bound although the molecule did not yet unbind from the surface. These terminal τ are shown with open circles in Figure 3. We present the data of τ as a function of the average number of OH groups bound in the corresponding time interval where, $n_{OH} = \frac{\sum_{t1}^{t2} N_{OH}}{t2 - t1}$, and $t2$ and $t1$ are the start and end points of the periods that are signaled by $N_{OH} = 0$

Calculation of Distribution of Lengths of Binding Blocks in Statistical Copolymers. We compute the distribution of lengths L

https://dx.doi.org/10.1021/jacs.9b12943
J. Am. Chem. Soc. 2020, 142, 4356−4366

of PVA blocks in random copolymers of vinyl alcohol and vinyl acetate monomers using a numerical model that accepts the incorporation of an acetylated monomer by comparing a uniformly distributed random number r between 0 and 1 to the fraction of acetylated monomers f_a in the polymer: if $r < f_a$ we add a vinyl acetate monomer, otherwise a vinyl alcohol one. We then measure the lengths of the PVA blocks for each polymer generated. The analysis of Figure 6 is performed with the data collected from 100000 independent realizations of polymers with DP_{total} = 351 to compare with the experiments of reference 33. SI Figure S9 shows the results of polymers of different lengths, from DP_{total} = 100 to 10000.

■ ASSOCIATED CONTENT

Supporting Information

The Supporting Information is available free of charge at https://pubs.acs.org/doi/10.1021/jacs.9b12943.

Time evolution of number of bound N_{OH} for 20 simulation trajectories for DP = 10, 15, and 20; time evolution of bound N_{OH} per PVA segment for PVA functionalized with 10% and 20% acetyl groups, respectively; time evolution of the dihedrals for a pure alkyl chain and a chain that includes an acetylated carbon; time evolution of the N_{OH} for a 10% dehydroxylated PVA chain for 20 representative simulation trajectories; probability of finding an acetylated group for a 10% acetylated PVA of DP = 351; probability $P(L)$ of finding a PVA block of length L in the randomly acetylated polymer and distribution of the most probable length of uninterrupted PVA block, $L \times P(L)$ for polymers of different DP and all with 10% acetylation (PDF)

■ AUTHOR INFORMATION

Corresponding Author

Valeria Molinero − *Department of Chemistry, The University of Utah, Salt Lake City, Utah 84112-0850, United States;* orcid.org/0000-0002-8577-4675; Email: Valeria.Molinero@utah.edu

Author

Pavithra M. Naullage − *Department of Chemistry, The University of Utah, Salt Lake City, Utah 84112-0850, United States*

Complete contact information is available at: https://pubs.acs.org/10.1021/jacs.9b12943

Notes

The authors declare no competing financial interest.

■ ACKNOWLEDGMENTS

We gratefully acknowledge discussions with Baron Peters, Ido Braslavsky, Thomas Koop, and Kenji Mochizuki. We thank the National Science Foundation for support of this work through award CHE-1305427 and the Center for High Performance Computing at the University of Utah for technical support and a grant of computing time.

■ REFERENCES

(1) Tyshenko, M. G.; Doucet, D.; Davies, P. L.; Walker, V. K. The antifreeze potential of the spruce budworm thermal hysteresis protein. *Nat. Biotechnol.* **1997**, *15*, 887−890.

(2) Davies, P. L.; Baardsnes, J.; Kuiper, M. J.; Walker, V. K. Structure and function of antifreeze proteins. *Philos. Trans. R. Soc., B* **2002**, *357*, 927−935.

(3) Sally, O. Y.; Brown, A.; Middleton, A. J.; Tomczak, M. M.; Walker, V. K.; Davies, P. L. Ice restructuring inhibition activities in antifreeze proteins with distinct differences in thermal hysteresis. *Cryobiology* **2010**, *61*, 327−334.

(4) Celik, Y.; Graham, L. A.; Mok, Y.-F.; Bar, M.; Davies, P. L.; Braslavsky, I. Superheating of ice crystals in antifreeze protein solutions. *Proc. Natl. Acad. Sci. U. S. A.* **2010**, *107*, 5423−5428.

(5) Bar Dolev, M.; Braslavsky, I.; Davies, P. L. Ice-binding proteins and their function. *Annu. Rev. Biochem.* **2016**, *85*, 515−542.

(6) Gilbert, J. A.; Davies, P. L.; Laybourn-Parry, J. A hyperactive, Ca2+-dependent antifreeze protein in an Antarctic bacterium. *FEMS Microbiol. Lett.* **2005**, *245*, 67−72.

(7) Voets, I. K. From ice-binding proteins to bio-inspired antifreeze materials. *Soft Matter* **2017**, *13*, 4808−4823.

(8) Surís-Valls, R.; Voets, I. K. Peptidic Antifreeze Materials: Prospects and Challenges. *Int. J. Mol. Sci.* **2019**, *20*, 5149.

(9) Harding, M. M.; Anderberg, P. I.; Haymet, A. D. J. 'Antifreeze' glycoproteins from polar fish. *Eur. J. Biochem.* **2003**, *270*, 1381−1392.

(10) Payne, S.; Sandford, D.; Harris, A.; Young, O. The effects of antifreeze proteins on chilled and frozen meat. *Meat Sci.* **1994**, *37*, 429−438.

(11) Gwak, Y.; Park, J.-i.; Kim, M.; Kim, H. S.; Kwon, M. J.; Oh, S. J.; Kim, Y.-P.; Jin, E. Creating anti-icing surfaces via the direct immobilization of antifreeze proteins on aluminum. *Sci. Rep.* **2015**, *5*, 12019.

(12) Lv, J.; Song, Y.; Jiang, L.; Wang, J. Bio-Inspired Strategies for Anti-Icing. *ACS Nano* **2014**, *8*, 3152−3169.

(13) Griffith, M.; Ewart, K. V. Antifreeze proteins and their potential use in frozen foods. *Biotechnol. Adv.* **1995**, *13*, 375−402.

(14) Mazur, P. Freezing of living cells: mechanisms and implications. *Am. J. Physiol., Cell Physiol.* **1984**, *247*, C125−C142.

(15) Arav, A.; Rubinsky, B.; Fletcher, G.; Seren, E. Cryogenic protection of oocytes with antifreeze proteins. *Mol. Reprod. Dev.* **1993**, *36*, 488−493.

(16) Petzold, G.; Aguilera, J. M. Ice morphology: fundamentals and technological applications in foods. *Food Biophys.* **2009**, *4*, 378−396.

(17) Berendsen, T. A.; Bruinsma, B. G.; Puts, C. F.; Saeidi, N.; Usta, O. B.; Uygun, B. E.; Izamis, M.-L.; Toner, M.; Yarmush, M. L.; Uygun, K. Supercooling enables long-term transplantation survival following 4 days of liver preservation. *Nat. Med.* **2014**, *20*, 790−793.

(18) Lifshitz, I. M.; Slyozov, V. V. The kinetics of precipitation from supersaturated solid solutions. *J. Phys. Chem. Solids* **1961**, *19*, 35−50.

(19) Budke, C.; Koop, T. Ice Recrystallization Inhibition and Molecular Recognition of Ice Faces by Poly(vinyl alcohol). *ChemPhysChem* **2006**, *7*, 2601−2606.

(20) Olijve, L. L.; Meister, K.; DeVries, A. L.; Duman, J. G.; Guo, S.; Bakker, H. J.; Voets, I. K. Blocking rapid ice crystal growth through nonbasal plane adsorption of antifreeze proteins. *Proc. Natl. Acad. Sci. U. S. A.* **2016**, *113*, 3740−3745.

(21) Lee, J.; Lee, S. Y.; Lim, D.-K.; Ahn, D. J.; Lee, S. Antifreezing Gold Colloids. *J. Am. Chem. Soc.* **2019**, *141*, 18682−18693.

(22) Rahman, A. T.; Arai, T.; Yamauchi, A.; Miura, A.; Kondo, H.; Ohyama, Y.; Tsuda, S. Ice recrystallization is strongly inhibited when antifreeze proteins bind to multiple ice planes. *Sci. Rep.* **2019**, *9*, 2212.

(23) Garnham, C. P.; Campbell, R. L.; Davies, P. L. Anchored clathrate waters bind antifreeze proteins to ice. *Proc. Natl. Acad. Sci. U. S. A.* **2011**, *108*, 7363−7367.

(24) Naullage, P. M.; Qiu, Y.; Molinero, V. What Controls the Limit of Supercooling and Superheating of Pinned Ice Surfaces? *J. Phys. Chem. Lett.* **2018**, *9*, 1712−1720.

(25) Karlsson, J. O.; Braslavsky, I.; Elliott, J. A. Protein−water−ice contact angle. *Langmuir* **2019**, *35*, 7383−7387.

(26) Mochizuki, K.; Qiu, Y.; Molinero, V. Promotion of homogeneous ice nucleation by soluble molecules. *J. Am. Chem. Soc.* **2017**, *139*, 17003−17006.

(27) Chasnitsky, M.; Braslavsky, I. Ice-binding proteins and the applicability and limitations of the kinetic pinning model. *Philos. Trans. R. Soc., A* **2019**, *377*, 20180391.

(28) Johnston, J. C.; Molinero, V. Crystallization, melting, and structure of water nanoparticles at atmospherically relevant temperatures. *J. Am. Chem. Soc.* **2012**, *134*, 6650−6659.
(29) Montero de Hijes, P.; Espinosa, J.; Vega, C.; Sanz, E. Ice growth rate: Temperature dependence and effect of heat dissipation. *J. Chem. Phys.* **2019**, *151*, No. 044509.
(30) Pruppacher, H. Interpretation of experimentally determined growth rates of ice crystals in supercooled water. *J. Chem. Phys.* **1967**, *47*, 1807−1813.
(31) Yagasaki, T.; Matsumoto, M.; Tanaka, H. Molecular Dynamics Study of Kinetic Hydrate Inhibitors: The Optimal Inhibitor Size and Effect of Guest Species. *J. Phys. Chem. C* **2019**, *123*, 1806−1816.
(32) Budke, C.; Dreyer, A.; Jaeger, J.; Gimpel, K.; Berkemeier, T.; Bonin, A. S.; Nagel, L.; Plattner, C.; DeVries, A. L.; Sewald, N. Quantitative efficacy classification of ice recrystallization inhibition agents. *Cryst. Growth Des.* **2014**, *14*, 4285−4294.
(33) Congdon, T.; Notman, R.; Gibson, M. I. Antifreeze (Glyco)protein Mimetic Behavior of Poly(vinyl alcohol): Detailed Structure Ice Recrystallization Inhibition Activity Study. *Biomacromolecules* **2013**, *14*, 1578−1586.
(34) Deller, R. C.; Vatish, M.; Mitchell, D. A.; Gibson, M. I. Synthetic polymers enable non-vitreous cellular cryopreservation by reducing ice crystal growth during thawing. *Nat. Commun.* **2014**, *5*, 3244.
(35) Knight, C. A.; Wen, D.; Laursen, R. A. Nonequilibrium Antifreeze Peptides and the Recrystallization of Ice. *Cryobiology* **1995**, *32*, 23−34.
(36) DeMerlis, C.; Schoneker, D. Review of the oral toxicity of polyvinyl alcohol (PVA). *Food Chem. Toxicol.* **2003**, *41*, 319−326.
(37) Hasan, M.; Fayter, A. E.; Gibson, M. I. Ice Recrystallization Inhibiting Polymers Enable Glycerol-Free Cryopreservation of Microorganisms. *Biomacromolecules* **2018**, *19*, 3371−3376.
(38) Naullage, P. M.; Lupi, L.; Molinero, V. Molecular Recognition of Ice by Fully Flexible Molecules. *J. Phys. Chem. C* **2017**, *121*, 26949−26957.
(39) Weng, L.; Stott, S. L.; Toner, M. Molecular dynamics at the interface between ice and poly (vinyl alcohol) and ice recrystallization inhibition. *Langmuir* **2018**, *34*, 5116−5123.
(40) Yeh, Y.; Feeney, R. E. Antifreeze Proteins: Structures and Mechanisms of Function. *Chem. Rev.* **1996**, *96*, 601−618.
(41) Lu, S.-S.; Inada, T.; Yabe, A.; Zhang, X.; Grandum, S. Microscale study of poly (vinyl alcohol) as an effective additive for inhibiting recrystallization in ice slurries. *Int. J. Refrig.* **2002**, *25*, 562−568.
(42) Stubbs, C.; Wilkins, L. E.; Fayter, A. E. R.; Walker, M.; Gibson, M. I. Multivalent Presentation of Ice Recrystallization Inhibiting Polymers on Nanoparticles Retains Activity. *Langmuir* **2019**, *35*, 7347−7353.
(43) Gibson, M. I. Slowing the growth of ice with synthetic macromolecules: beyond antifreeze(glyco) proteins. *Polym. Chem.* **2010**, *1*, 1141−1152.
(44) Raymond, J. A.; DeVries, A. L. Adsorption inhibition as a mechanism of freezing resistance in polar fishes. *Proc. Natl. Acad. Sci. U. S. A.* **1977**, *74*, 2589−2593.
(45) Stubbs, C.; Congdon, T. R.; Gibson, M. I. Photo-polymerisation and study of the ice recrystallisation inhibition of hydrophobically modified poly (vinyl pyrrolidone) co-polymers. *Eur. Polym. J.* **2019**, *110*, 330−336.
(46) Deller, R. C.; Congdon, T.; Sahid, M. A.; Morgan, M.; Vatish, M.; Mitchell, D. A.; Notman, R.; Gibson, M. I. Ice recrystallisation inhibition by polyols: comparison of molecular and macromolecular inhibitors and role of hydrophobic units. *Biomater. Sci.* **2013**, *1*, 478−485.
(47) Capicciotti, C. J.; Leclere, M.; Perras, F. A.; Bryce, D. L.; Paulin, H.; Harden, J.; Liu, Y.; Ben, R. N. Potent inhibition of ice recrystallization by low molecular weight carbohydrate-based surfactants and hydrogelators. *Chem. Sci.* **2012**, *3*, 1408−1416.
(48) Hudait, A.; Odendahl, N.; Qiu, Y.; Paesani, F.; Molinero, V. Ice Nucleating and Antifreeze Proteins Recognize Ice Through a Diversity of Anchored Clathrate and Ice-Like Motifs. *J. Am. Chem. Soc.* **2018**, *140*, 4905−4912.
(49) Kuiper, M. J.; Morton, C. J.; Abraham, S. E.; Gray-Weale, A. The biological function of an insect antifreeze protein simulated by molecular dynamics. *eLife* **2015**, *4*, No. e05142.
(50) Hudait, A.; Moberg, D. R.; Qiu, Y.; Odendahl, N.; Paesani, F.; Molinero, V. Preordering of water is not needed for ice recognition by hyperactive antifreeze proteins. *Proc. Natl. Acad. Sci. U. S. A.* **2018**, *115*, 8266−8271.
(51) Qiu, Y.; Odendahl, N.; Hudait, A.; Mason, R.; Bertram, A. K.; Paesani, F.; DeMott, P. J.; Molinero, V. Ice nucleation efficiency of hydroxylated organic surfaces is controlled by their structural fluctuations and mismatch to ice. *J. Am. Chem. Soc.* **2017**, *139*, 3052−3064.
(52) Mochizuki, K.; Molinero, V. Antifreeze glycoproteins bind reversibly to ice via hydrophobic groups. *J. Am. Chem. Soc.* **2018**, *140*, 4803−4811.
(53) Inada, T.; Lu, S.-S. Thermal hysteresis caused by non-equilibrium antifreeze activity of poly(vinyl alcohol). *Chem. Phys. Lett.* **2004**, *394*, 361−365.
(54) Sander, L. M.; Tkachenko, A. V. Kinetic pinning and biological antifreezes. *Phys. Rev. Lett.* **2004**, *93*, 128102.
(55) Molinero, V.; Moore, E. B. Water Modeled As an Intermediate Element between Carbon and Silicon. *J. Phys. Chem. B* **2009**, *113*, 4008−4016.
(56) Congdon, T. R.; Notman, R.; Gibson, M. I. Influence of Block Copolymerization on the Antifreeze Protein Mimetic Ice Recrystallization Inhibition Activity of Poly (vinyl alcohol). *Biomacromolecules* **2016**, *17*, 3033−3039.
(57) Ampaw, A.; Charlton, T. A.; Briard, J. G.; Ben, R. N. Designing the next generation of cryoprotectants−From proteins to small molecules. *J. Pept. Sci.* **2019**, *111*, No. e24086.
(58) Tachibana, Y.; Fletcher, G. L.; Fujitani, N.; Tsuda, S.; Monde, K.; Nishimura, S. I. Antifreeze glycoproteins: elucidation of the structural motifs that are essential for antifreeze activity. *Angew. Chem., Int. Ed.* **2004**, *43*, 856−862.
(59) Waldow, D. A.; Johnson, B. S.; Hyde, P. D.; Ediger, M.; Kitano, T.; Ito, K. Local segmental dynamics of polyisoprene in dilute solution: solvent and molecular weight effects. *Macromolecules* **1989**, *22*, 1345−1351.
(60) Hudait, A.; Qiu, Y.; Odendahl, N.; Molinero, V. Hydrogen-Bonding and Hydrophobic Groups Contribute Equally to the Binding of Hyperactive Antifreeze and Ice Nucleating Proteins to Ice. *J. Am. Chem. Soc.* **2019**, *141*, 7887−7898.
(61) Biggs, C. I.; Stubbs, C.; Graham, B.; Fayter, A. E.; Hasan, M.; Gibson, M. I. Mimicking the Ice Recrystallization Activity of Biological Antifreezes. When is a New Polymer "Active"? *Macromol. Biosci.* **2019**, 1900082.
(62) Telis, V. R. N.; Telis-Romero, J.; Mazzotti, H.; Gabas, A. L. Viscosity of aqueous carbohydrate solutions at different temperatures and concentrations. *Int. J. Food Prop.* **2007**, *10*, 185−195.
(63) Meister, K.; DeVries, A. L.; Bakker, H. J.; Drori, R. Antifreeze glycoproteins bind irreversibly to ice. *J. Am. Chem. Soc.* **2018**, *140*, 9365−9368.
(64) Liou, Y.-C.; Tocilj, A.; Davies, P. L.; Jia, Z. Mimicry of ice structure by surface hydroxyls and water of a beta-helix antifreeze protein. *Nature* **2000**, *406*, 322−324.
(65) Midya, U. S.; Bandyopadhyay, S. Hydration behavior at the ice-binding surface of the Tenebrio molitor antifreeze protein. *J. Phys. Chem. B* **2014**, *118*, 4743−4752.
(66) Marshall, C. B.; Daley, M. E.; Sykes, B. D.; Davies, P. L. Enhancing the activity of a β-helical antifreeze protein by the engineered addition of coils. *Biochemistry* **2004**, *43*, 11637−11646.
(67) Qiu, Y.; Hudait, A.; Molinero, V. How Size and Aggregation of Ice-binding Proteins Control their Ice Nucleation Efficiency. *J. Am. Chem. Soc.* **2019**, *141*, 7439−7452.
(68) Kamat, K.; Molinero, V.; Peters, B., in preparation.
(69) Plimpton, S. Fast parallel algorithms for short-range molecular dynamics. *J. Comput. Phys.* **1995**, *117*, 1−19.

https://dx.doi.org/10.1021/jacs.9b12943
J. Am. Chem. Soc. 2020, 142, 4356−4366

(70) Nosé, S. A unified formulation of the constant temperature molecular dynamics methods. *J. Chem. Phys.* **1984**, *81*, 511−519.
(71) Hoover, W. G. Canonical dynamics: equilibrium phase-space distributions. *Phys. Rev. A: At., Mol., Opt. Phys.* **1985**, *31*, 1695.
(72) Hudait, A.; Qiu, S.; Lupi, L.; Molinero, V. Free energy contributions and structural characterization of stacking disordered ices. *Phys. Chem. Chem. Phys.* **2016**, *18*, 9544−9553.
(73) Moore, E. B.; Molinero, V. Growing correlation length in supercooled water. *J. Chem. Phys.* **2009**, *130*, 244505.
(74) Moore, E. B.; Molinero, V. Is it cubic? Ice crystallization from deeply supercooled water. *Phys. Chem. Chem. Phys.* **2011**, *13*, 20008−20016.
(75) Lu, J.; Qiu, Y.; Baron, R.; Molinero, V. Coarse-Graining of TIP4P/2005, TIP4P-Ew, SPC/E, and TIP3P to Monatomic Anisotropic Water Models Using Relative Entropy Minimization. *J. Chem. Theory Comput.* **2014**, *10*, 4104−4120.
(76) Moore, E. B.; Molinero, V. Structural transformation in supercooled water controls the crystallization rate of ice. *Nature* **2011**, *479*, 506−8.
(77) Jacobson, L. C.; Kirby, R. M.; Molinero, V. How short is too short for the interactions of a water potential? Exploring the parameter space of a coarse-grained water model using uncertainty quantification. *J. Phys. Chem. B* **2014**, *118*, 8190−8202.
(78) Factorovich, M. H.; Molinero, V.; Scherlis, D. A. Vapor pressure of water nanodroplets. *J. Am. Chem. Soc.* **2014**, *136*, 4508−4514.
(79) Perez Sirkin, Y. A.; Factorovich, M. H.; Molinero, V.; Scherlis, D. A. Vapor Pressure of Aqueous Solutions of Electrolytes Reproduced with Coarse-Grained Models without Electrostatics. *J. Chem. Theory Comput.* **2016**, *12*, 2942−2949.
(80) Baron, R.; Molinero, V. Water-driven cavity−ligand binding: comparison of thermodynamic signatures from coarse-grained and atomic-level simulations. *J. Chem. Theory Comput.* **2012**, *8*, 3696−3704.
(81) Song, B.; Molinero, V. Thermodynamic and structural signatures of water-driven methane-methane attraction in coarse-grained mW water. *J. Chem. Phys.* **2013**, *139*, No. 054511.
(82) Jacobson, L. C.; Molinero, V. A Methane−Water Model for Coarse-Grained Simulations of Solutions and Clathrate Hydrates. *J. Phys. Chem. B* **2010**, *114*, 7302−7311.
(83) Nguyen, A. H.; Koc, M. A.; Shepherd, T. D.; Molinero, V. Structure of the Ice−Clathrate Interface. *J. Phys. Chem. C* **2015**, *119*, 4104−4117.
(84) Qiu, Y.; Molinero, V. Morphology of Liquid−Liquid Phase Separated Aerosols. *J. Am. Chem. Soc.* **2015**, *137*, 10642−10651.
(85) Lupi, L.; Molinero, V. Does hydrophilicity of carbon particles improve their ice nucleation ability? *J. Phys. Chem. A* **2014**, *118*, 7330−7337.
(86) Shepherd, T. D.; Koc, M. A.; Molinero, V. The quasi-liquid layer of ice under conditions of methane clathrate formation. *J. Phys. Chem. C* **2012**, *116*, 12172−12180.
(87) Qiu, Y.; Lupi, L.; Molinero, V. Is Water at the Graphite Interface Vapor-Like or Ice-Like? *J. Phys. Chem. B* **2018**, *122*, 3626−3634.
(88) Qiu, Y.; Molinero, V. Why Is It So Difficult to Identify the Onset of Ice Premelting? *J. Phys. Chem. Lett.* **2018**, *9*, 5179−5182.
(89) Factorovich, M. H.; Naullage, P. M.; Molinero, V. Can clathrates heterogeneously nucleate ice? *J. Chem. Phys.* **2019**, *151*, 114707.
(90) Naullage, P. M.; Bertolazzo, A. A.; Molinero, V. How Do Surfactants Control the Agglomeration of Clathrate Hydrates? *ACS Cent. Sci.* **2019**, *5*, 428−439.
(91) Nguyen, A. H.; Jacobson, L. C.; Molinero, V. Structure of the Clathrate/Solution Interface and Mechanism of Cross-Nucleation of Clathrate Hydrates. *J. Phys. Chem. C* **2012**, *116*, 19828−19838.
(92) Bertolazzo, A. A.; Naullage, P. M.; Peters, B.; Molinero, V. The Clathrate−Water Interface Is Oleophilic. *J. Phys. Chem. Lett.* **2018**, *9*, 3224−3231.
(93) Lupi, L.; Kastelowitz, N.; Molinero, V. Vapor deposition of water on graphitic surfaces: Formation of amorphous ice, bilayer ice, ice I, and liquid water. *J. Chem. Phys.* **2014**, *141*, 18C508.
(94) Perez Sirkin, Y. A.; Gadea, E. D.; Scherlis, D. A.; Molinero, V. Mechanisms of Nucleation and Stationary States of Electrochemically Generated Nanobubbles. *J. Am. Chem. Soc.* **2019**, *141*, 10801−10811.
(95) Malkin, T. L.; Murray, B. J.; Salzmann, C. G.; Molinero, V.; Pickering, S. J.; Whale, T. F. Stacking disorder in ice I. *Phys. Chem. Chem. Phys.* **2015**, *17*, 60−76.
(96) Moore, E. B.; De La Llave, E.; Welke, K.; Scherlis, D. A.; Molinero, V. Freezing, melting and structure of ice in a hydrophilic nanopore. *Phys. Chem. Chem. Phys.* **2010**, *12*, 4124−4134.
(97) Kastelowitz, N.; Johnston, J. C.; Molinero, V. The anomalously high melting temperature of bilayer ice. *J. Chem. Phys.* **2010**, *132*, 124511.
(98) Moore, E. B.; Molinero, V. Ice crystallization in water's "no-man's land. *J. Chem. Phys.* **2010**, *132*, 244504.
(99) Moore, E. B.; Allen, J. T.; Molinero, V. Liquid-ice coexistence below the melting temperature for water confined in hydrophilic and hydrophobic nanopores. *J. Phys. Chem. C* **2012**, *116*, 7507−7514.
(100) Bullock, G.; Molinero, V. Low-density liquid water is the mother of ice: on the relation between mesostructure, thermodynamics and ice crystallization in solutions. *Faraday Discuss.* **2014**, *167*, 371−388.
(101) Le, L.; Molinero, V. Nanophase segregation in supercooled aqueous solutions and their glasses driven by the polyamorphism of water. *J. Phys. Chem. A* **2011**, *115*, 5900−5907.
(102) Johnston, J. C.; Kastelowitz, N.; Molinero, V. Liquid to quasicrystal transition in bilayer water. *J. Chem. Phys.* **2010**, *133*, 154516.
(103) Jacobson, L. C.; Hujo, W.; Molinero, V. Thermodynamic Stability and Growth of Guest-Free Clathrate Hydrates: A Low-Density Crystal Phase of Water. *J. Phys. Chem. B* **2009**, *113*, 10298−10307.
(104) Jacobson, L. C.; Hujo, W.; Molinero, V. Nucleation Pathways of Clathrate Hydrates: Effect of Guest Size and Solubility. *J. Phys. Chem. B* **2010**, *114*, 13796−13807.
(105) Jacobson, L. C.; Hujo, W.; Molinero, V. Amorphous precursors in the nucleation of clathrate hydrates. *J. Am. Chem. Soc.* **2010**, *132*, 11806−11811.
(106) Jacobson, L. C.; Molinero, V. Can amorphous nuclei grow crystalline clathrates? The size and crystallinity of critical clathrate nuclei. *J. Am. Chem. Soc.* **2011**, *133*, 6458−6463.
(107) Nguyen, A. H.; Molinero, V. Cross-nucleation between clathrate hydrate polymorphs: Assessing the role of stability, growth rate, and structure matching. *J. Chem. Phys.* **2014**, *140*, No. 084506.
(108) Song, B.; Nguyen, A. H.; Molinero, V. Can Guest Occupancy in Binary Clathrate Hydrates Be Tuned through Control of the Growth Temperature? *J. Phys. Chem. C* **2014**, *118*, 23022−23031.
(109) Moberg, D. R.; Becker, D.; Dierking, C. W.; Zurheide, F.; Bandow, B.; Buck, U.; Hudait, A.; Molinero, V.; Paesani, F.; Zeuch, T. The end of ice I. *Proc. Natl. Acad. Sci. U. S. A.* **2019**, *116*, 24413−24419.
(110) Xu, L.; Molinero, V. Liquid− Vapor Oscillations of Water Nanoconfined between Hydrophobic Disks: Thermodynamics and Kinetics. *J. Phys. Chem. B* **2010**, *114*, 7320−7328.
(111) Xu, L.; Molinero, V. Is There a Liquid−Liquid Transition in Confined Water? *J. Phys. Chem. B* **2011**, *115*, 14210−14216.
(112) De La Llave, E.; Molinero, V.; Scherlis, D. A. Water filling of hydrophilic nanopores. *J. Chem. Phys.* **2010**, *133*, No. 034513.
(113) Lupi, L.; Hanscam, R.; Qiu, Y.; Molinero, V. Reaction Coordinate for Ice Crystallization on a Soft Surface. *J. Phys. Chem. Lett.* **2017**, *8*, 4201−4205.
(114) Nguyen, A. H.; Molinero, V. Identification of Clathrate Hydrates, Hexagonal Ice, Cubic Ice, and Liquid Water in Simulations: the CHILL+ Algorithm. *J. Phys. Chem. B* **2015**, *119*, 9369−9376.

https://dx.doi.org/10.1021/jacs.9b12943
J. Am. Chem. Soc. 2020, 142, 4356−4366